Protein Science (1996), 5:1648–1654. Cambridge University Press. Printed in the USA.

Role of the divalent metal ion in the NAD:malic enzyme reaction: An ESEEM determination of the ground state conformation of malate in the E:Mn:malate complex

PETER A. TIPTON,[1] THOMAS P. QUINN,[1] JACK PEISACH,[2] AND PAUL F. COOK[3]

[1] Department of Biochemistry, University of Missouri-Columbia, Columbia, Missouri 65211
[2] Department of Physiology and Biophysics, Albert Einstein College of Medicine, Bronx, New York 10461
[3] Department of Biochemistry and Molecular Biology, University of North Texas Health Science Center at Fort Worth, Fort Worth, Texas 76107

(RECEIVED February 7, 1996; ACCEPTED May 14, 1996)

Abstract

The conformation of L-malate bound at the active site of *Ascaris suum* malic enzyme has been investigated by electron spin echo envelope modulation spectroscopy. Dipolar interactions between Mn^{2+} bound to the enzyme active site and deuterium specifically placed at the 2-position, the 3*R*-position, and the 3*S*-position of L-malate were observed. The intensities of these interactions are related to the distance between each deuterium and Mn^{2+}. Several models of possible Mn-malate complexes were constructed using molecular graphics techniques, and conformational searches were conducted to identify conformers of malate that meet the distance criteria defined by the spectroscopic measurements. These searches suggest that L-malate binds to the enzyme active site in the *trans* conformation, which would be expected to be the most stable conformer in solution, not in the *gauche* conformer, which would be more similar to the conformation required for oxidative decarboxylation of oxalacetate formed from L-malate at the active site of the enzyme.

Keywords: decarboxylation; EPR spectroscopy; malic enzyme; substrate conformation

The mitochondrial NAD-malic enzyme (EC 1.1.1.39) from *Ascaris suum* catalyzes the divalent metal ion-dependent oxidative decarboxylation of L-malate utilizing NAD to yield pyruvate, CO_2, and NADH. Several different divalent metal ions including Mg^{2+}, Mn^{2+}, Co^{2+}, Ni^{2+}, Cd^{2+}, and Zn^{2+} (Schimerlik et at., 1977; Grissom & Cleland, 1988) have been shown to support catalysis in the NADP-malic enzyme from chicken liver and in the NAD-malic enzyme from *A. suum* (Karsten et al., 1995). The kinetic mechanism is steady-state random with the requirement that the divalent metal ion bind prior to L-malate (Park et al., 1984; Chen et al., 1988).

A stepwise oxidative decarboxylation of malate by the NADP-malic enzyme was proposed early in the investigation of its mechanism (Viega Salles & Ochoa, 1950; Hsu, 1970; Tang & Hsu, 1973) with hydride transfer from malate to NADP preceding decarboxylation of the resulting oxalacetate intermediate. The proposed mechanism was based on the observation that the NADP-enzyme will catalyze the reduction of oxalacetate to malate and the decarboxylation of oxalacetate to pyruvate and CO_2 in the presence of NADPH. Similar conclusions were reached for the NAD-malic enzyme based on catalysis of the decarboxylation of oxalacetate in the absence and presence of NAD (Park et al., 1986). The stepwise oxidative decarboxylation mechanism with NAD(P) as the dinucleotide reactant is supported by multiple isotope effect studies (Hermes et al., 1982; Weiss et al., 1991) and partitioning of the E·NAD(P)H·metal·

Reprint requests to: Peter A. Tipton, Department of Biochemistry, University of Missouri-Columbia, 117 Schweitzer Hall, Columbia, Missouri 65211; e-mail: muccgw.bctipton@ssgate.missouri.edu; or Paul F. Cook, Department of Biochemistry and Molecular Biology, University of North Texas Health Science Center at Fort Worth, Fort Worth, Texas 76107; e-mail: pcook@jove.acs.unt.edu.

Abbreviations: DTT, dithiothreitol; EDTA, ethylenediaminetetraacetic acid; ESEEM, electron spin echo envelope modulation spectroscopy; HEPES, *N*-(2-hydroxyethyl)piperazine-*N*′-2-ethanesulfonic acid; MES, 2-(*N*-morpholino)ethanesulfonic acid; Tris, tris(hydroxymethyl)aminomethane: MDH, malate dehydrogenase; NAD, nicotinamide adenine dinucleotide (the + charge is omitted for convenience); NADP, nicotinamide adenine dinucleotide 2′-phosphate; APAD, 3-acetylpyridine adenine dinucleotide; PAAD, 3-pyridinealdehyde adenine dinucleotide.

oxalacetate complex (Hermes et al., 1982; Grissom & Cleland, 1988; Karsten & Cook, 1994; Karsten et al., 1995).[4]

The nonenzymatic decarboxylation of oxalacetate catalyzed by several different divalent metal ions proceeds with nearly equal ^{13}C isotope effects of about 1.05 (Grissom & Cleland, 1986), and these effects are equal to the intrinsic ^{13}C isotope effect of 1.05 estimated for the NAD(P)-malic enzyme catalyzed oxidative decarboxylation of malate with Mg^{2+} as the metal ion activator (Hermes et al., 1982; Grissom & Cleland, 1985; Karsten & Cook, 1994). As a result, the metal ion has been proposed to act as a Lewis acid positioned near the carbonyl of the oxalacetate intermediate to facilitate decarboxylation (Grissom & Cleland, 1988).

More recently, Karsten et al. (1995) have used deuterium, tritium, and ^{13}C primary kinetic isotope effects, and the enzyme-catalyzed partitioning of oxalacetate to pyruvate and malate, with several different divalent metal ions to probe the role of the metal ion in the hydride transfer step that precedes the decarboxylation of the oxalacetate intermediate. With NAD as dinucleotide substrate, a direct correlation between the size of the divalent metal ion activator and the intrinsic deuterium isotope effect is observed. An isotope effect significantly greater than the semiclassical limit is calculated when Cd^{2+} is the metal ion activator, suggesting a substantial tunneling contribution. The primary intrinsic ^{13}C isotope effect on the decarboxylation step increases over the series $Mg^{2+} < Mn^{2+} < Cd^{2+}$, which is in contrast to the equal isotope effects measured for these metal ions for the nonenzymatic decarboxylation of oxalacetate (Grissom & Cleland, 1985). A survey of malate inhibitory analogues shows that the enzyme is inhibited by analogues with various functional group substitutions at the β-carbon and also indicates that the metal ion provides a major determinant for substrate binding (Karsten et al., 1995).

The above discussion is consistent with the divalent metal ion binding in the proximity of the α-hydroxyl of malate. Indeed, a mechanism has been written with the divalent metal ion coordinated directly to the α-hydroxyl and α-carboxyl of L-malate (Kiick et al., 1986). However, Mildvan and his colleagues (Hsu et al., 1976), using the paramagnetic enhancement effect in the NMR with Mn^{2+} as the divalent metal ion and monitoring the E·Mn·pyruvate complex, have suggested that the divalent metal ion forms a second sphere complex with pyruvate; that is, a water molecule intervenes between Mn^{2+} and the carbonyl oxygen of pyruvate. In order to obtain additional information of the structure of the ground state complex of the malic enzyme with metal and L-malate, we have utilized ESEEM spectroscopy with Mn^{2+} as the divalent metal ion and L-malate specifically deuterated at the 2-, 3*S*-, and 3*R*-positions. These data allow us to assess the relative distances from Mn^{2+} to each protonic position, which serves to define the conformation of malate. It appears that the conformation in which malate is bound at the active site in this complex is similar to the low-energy conformation that malate would be expected to assume in solution. Furthermore, these data suggest that malate is not a bidentate ligand of Mn^{2+}, and is probably not an inner sphere ligand at all in the ternary E·Mn·malate complex.

Results

The Fourier-transformed ESEEM spectrum of the enzyme complex with unlabeled malate was essentially featureless, except for a peak at 14 MHz arising from incomplete suppression of proton modulations. The difference spectra obtained by dividing the E·Mn·malate spectra obtained with unlabeled malate into those obtained with the deuterated malates are shown in Figure 1. Each spectrum is characterized by a peak at 2.1 MHz, which is the Larmor frequency of ^{2}H under the experimental conditions used. The 2.1-MHz peak is consistent with ^{2}H be-

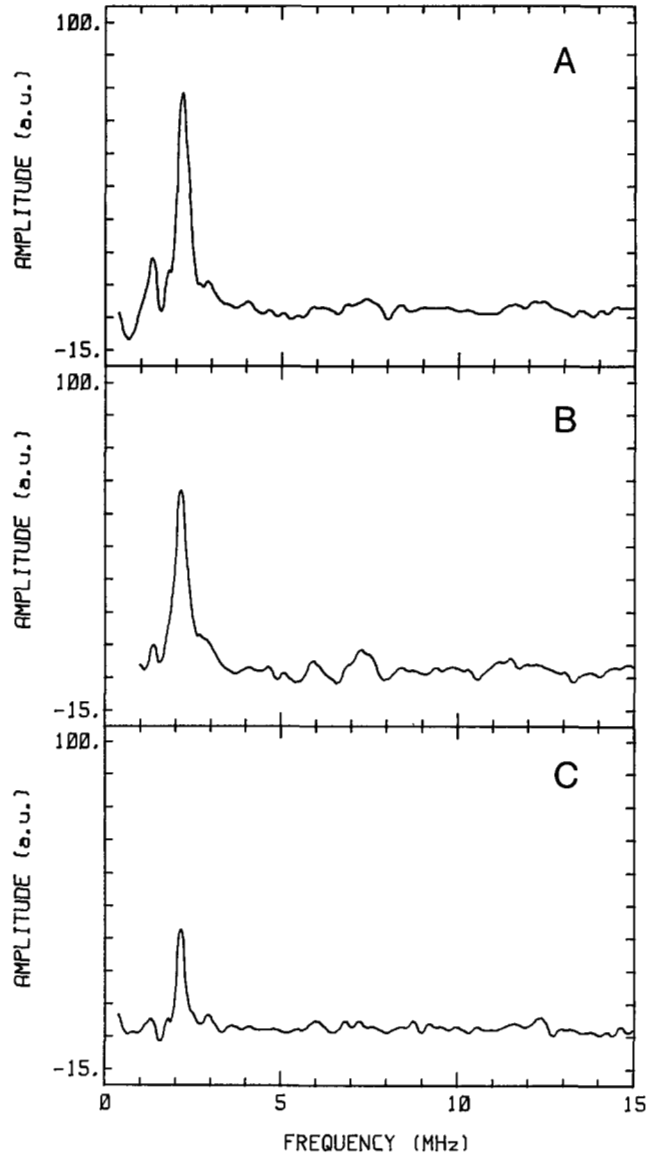

Fig. 1. ESEEM difference spectra of Mn-malate-malic enzyme complexes at $\tau = 145$ ns; other experimental conditions are given in the text. **A:** Mn-[2-^{2}H]malate-malic enzyme. **B:** Mn-[3*S*-^{2}H]malate-malic enzyme. **C:** Mn-[3*R*-^{2}H]malate-malic enzyme. The ESEEM spectrum of Mn-protio-malate-malic enzyme has been subtracted from each spectrum.

[4] The mechanism apparently changes from a sequential oxidative decarboxylation of L-malate with NAD(P) as the dinucleotide reactant to a concerted oxidative decarboxylation of L-malate with 3-APAD, 3-PAAD, or thioNAD as the dinucleotide reactant (Karsten & Cook, 1994; Karsten et al., 1995).

ing coupled to Mn(II) through dipolar interactions. There is no evidence for contact coupling in these spectra. Spectra obtained at different values of τ showed no significant differences from the ones shown in Figure 1. The peak at 1.3 MHz observable in Figure 1A is believed to arise from an artifact introduced by the dead-time reconstruction; this feature is not apparent in spectra obtained at different values of τ.

The magnetic interactions between Mn^{2+} and nuclei that are not coordinated directly to it can be approximated satisfactorily by treating them as classical magnetic dipole interactions (Metz et al., 1982; Larsen et al., 1992). In the above treatment, the depth of the modulations in the ESE envelope and the height of the corresponding peak in the Fourier-transformed spectrum is proportional to $1/r^6$, where r is the distance between the nuclear and electron spins (Mims & Peisach, 1981). The relative intensities of the ^2H Larmor peak in the spectra in Figure 1, which were obtained with [2-^{2}H]malate, [3*S*-^{2}H]malate, and [3*R*-^{2}H]malate, were 80:67:37. Therefore, the distances between Mn and H2, H3*S*, and H3*R* are in the ratio of 1:1.03:1.14. Analysis of another set of data obtained with $\tau = 217$ ns yielded distance ratios for Mn and H2, H3*S*, and H3*R* of 1:1.04:1.16.

The inverse sixth power relationship between distance and peak height suggests that distance measurements will be relatively insensitive to errors in peak height measurement. In fact, a 5% variation in opposite directions of the peak heights of any two peaks defines a range of intensities of 1:1.01–1.05:1.12–1.16 for the relative distances between H2, H3*S*, H3*R*, and Mn.

A search for Mn-malate conformations that would satisfy this relationship was conducted with each of the three models shown in Figure 2. In the first model (Fig. 2, left), the only rotatable bond whose movement would affect the Mn-^{2}H distances was the C2-C3 bond, which was rotated in 5° increments. No conformation that fulfilled the relative distance constraints was found. In the second model (Fig. 2, center), the C2-C3 bond was rotated, as was the bond connecting C2 and the hydroxyl oxygen. Again, no conformations were found that fulfilled the distance constraints defined above, although a single conformer in which the dihedral angle between the malate carboxyl groups was 90° was characterized by relative distances from Mn to H2, H3*S*, and H3*R* of 1:1.03:1.17.

A third search was conducted using the complex in which malate was hydrogen bonded through its hydroxyl group to a water molecule coordinated to Mn (Fig. 2, right). This outer sphere coordination model contains three rotatable bonds, which were varied systematically in 5° increments. The resulting conformers were screened to isolate those that fulfilled the relative distance criterion. From 54,000 possible conformers, 36 were identified. The 36 conformers fell into a relatively well-defined family; there was a large range of allowed values for RB3, which varied within a range of 120°. However, the angles around the C2-C3 bond and the C3-OH bond of malate were constrained fairly closely. The C2-C3 angles (RB1 in Fig. 2) fell within a range of 60°, and there were only four acceptable values for the C3-OH angle (RB2). The family of structures defined by these ranges is illustrated in Figure 3 (the Mn-O-H bond has been fixed in this illustration).

Discussion

Malic enzyme catalyzes the oxidative decarboxylation of L-malate; in the reaction with NAD as the cosubstrate, it seems clearly established that OAA is an intermediate that is formed prior to decarboxylation. There is a conformational prerequisite for decarboxylation of β-keto acids. In order to allow overlap between the orbitals in the labile C3-C4 bond and the incipient π bonds of the pyruvate enolate, OAA must be oriented so that the C3-C4 bond is orthogonal to the plane defined by the C2 carbonyl (Pollack, 1978). If the principle of least motion is adhered to (Thornton & Thornton, 1978), this arrangement would arise from a conformer of malate in which the carboxyl groups are in a *gauche* relationship with one another. Presumably, malate exists in solution in the more stable *trans* conformation, thus raising the question whether malic enzyme binds the more prevalent *trans* conformer of malate and adjusts its conformation at the active site, or whether it selects those molecules in the required *gauche* conformation. Kinetic studies have established that free malate is the species that binds to the enzyme, not the M^{2+}-malate complex (Park et al., 1984).

We have examined the conformation of malate bound at the active site of malic enzyme using ESEEM spectroscopy. The determination of the conformations of small, flexible molecules bound to macromolecules presents unique problems. Measurement of intramolecular NOEs is a potential approach, although the number of conformation-defining distance constraints can be small for a molecule with few protons. A more serious problem is that, in flexible molecules in which there is no known fixed distance that can be used as an internal standard, the quantitative interpretation of intramolecular NOEs becomes challeng-

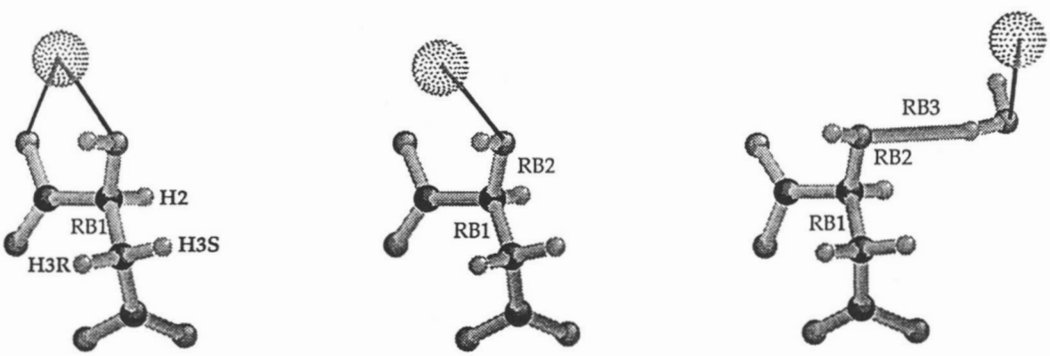

Fig. 2. For each of the three models shown, a search for Mn-malate conformations that would satisfy the inverse sixth power relationship between distance and peak height was conducted. The third model proved successful (see text).

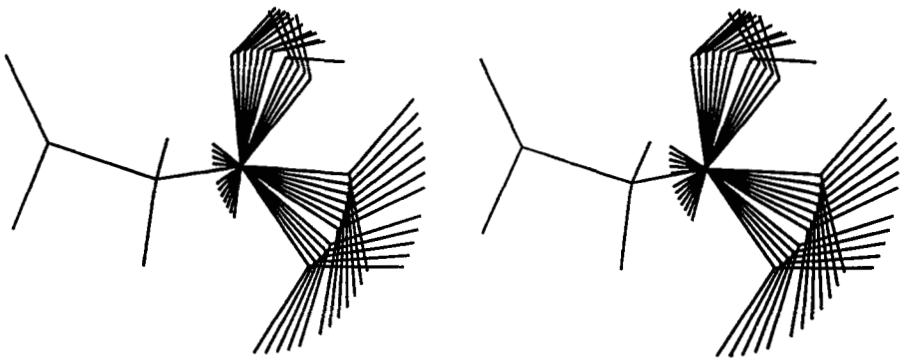

Fig. 3. Stereo representation of the conformations of malate that are consistent with the distance criteria established by the ESEEM data for an outer sphere Mn-malate complex. Mn and the water molecule intervening between Mn and malate have been omitted for clarity.

ing (Rosevear & Mildvan, 1989). For some systems, ESEEM spectroscopy offers an alternative to NOE measurements and paramagnetic perturbation techniques for distance determinations. For $S = 1/2$ systems, the methodology for spectral simulation, from which distances can be derived, is well established (Snetsinger et al., 1988). More recently, the treatment of $S > 1/2$ systems have been discussed, and distances have been calculated between Mn and nearby nuclei (Coffino & Peisach, 1992; Larsen et al., 1992). A simpler alternative to spectral simulation of complex systems is to use molecular modeling techniques with the relative distances that are defined by dipole-dipole interactions as constraints on the conformation. In the present case, distance constraints were generated by measuring Mn-^{2}H interactions with isotopomers of malate that had been deuterated at each of the three protonic sites in the molecule. The relative distances between each deuterium and Mn were used to screen possible conformations of Mn-malate complexes.

The assumptions made in the analysis of the ESEEM spectra are rather sweeping, but not unwarranted. First of all, it is apparent from the fact that the ^{2}H signal appears as an unsplit peak at the ^{2}H Larmor frequency that there is little, if any, contact coupling between Mn and ^{2}H. The dipolar nature of the interaction is not surprising considering the number of bonds separating the nuclei. Contact-coupled ^{2}H has been observed in biological systems, and yields spectra distinguished easily from those obtained in the present work; in metmyoglobin, ^{2}H from ^2H_2O coordinated directly to the heme iron appears in ESEEM spectra as a doublet with a 0.8-MHz coupling centered around the ^{2}H Larmor frequency (Peisach et al., 1984). Detailed studies of the Mn·N-*ras* p21·GDP complex, in which interatomic distances derived from crystallographic analysis and from ESEEM analysis were compared, validate the assumption that the weakly coupled nuclei can be treated as point dipoles (Larsen et al., 1992, 1993). We have not attempted to correct for the fact that deuterium is a quadrupolar nucleus; Mims et al. (1977) estimated that neglecting the quadrupolar interaction would lead to no more than a 10% underestimate of interatomic distances. Such "worst cases" occur when there is a significant degree of covalent bonding between the metal and the ligand, which is not the case in the present study. Even in the absence of correction for the quadrupolar interactions, ESEEM-derived relative distances between Fe^{3+} and deuteria at the active site of cytochrome *c* are in excellent agreement with crystallographically derived values (Mims et al., 1990).

The analysis of the active site complex is potentially complicated by the fact that the position of Mn^{2+} relative to malate has not been established. However, it is well established that the role of the divalent metal ion in enzyme-catalyzed oxidative decarboxylations is to provide an electron sink to facilitate decarboxylation of the β-keto acid (Steinberger & Westheimer, 1951). Thus, we examined the three model complexes shown in Figure 2, all of which would allow Mn^{2+} to fulfill its role in the catalytic reaction. In the first two complexes, malate is an inner sphere ligand of Mn^{2+}; coordination occurs through the C1 carboxyl group and the C2 hydroxyl group in the first complex, and only through the hydroxyl group in the second complex. In the third complex examined, malate is treated as an outer sphere ligand of Mn^{2+}.

The first inner sphere complex contains only one rotatable bond whose variation changes the distances between Mn^{2+} and the three protonic sites of malate. A systematic search of all the conformations generated by rotation around that bond determined that none of the resulting conformations fulfilled the relative distance constraints from the ESEEM data. In this model, if malate assumed the conformation required for generating OAA oriented properly for decarboxylation, the relative distances from Mn to H2, H3*S*, and H3*R* are predicted to be 1:1.07:1.06. It is clear that the data are not consistent with this scenario.

We therefore examined the second inner sphere complex, in which malate is coordinated to Mn^{2+} solely through the hydroxyl group oxygen. This complex has two rotatable bonds, and their variation again failed to yield a conformation in which the relative Mn-^{2}H distances fell within the range defined by the ESEEM spectra.

In an attempt to find a satisfactory conformational solution to the ESEEM data, we constructed a model in which a water molecule intervened between Mn and malate. In fact, early NMR studies of pigeon liver malic enzyme were interpreted to suggest that malate was a second sphere ligand of Mn (Hsu et al., 1976). The outer sphere complex has three rotatable bonds, which were varied in 5° increments in the conformational search to define 54,000 unique conformers. However, only a small subset of these contained Mn-proton distances that ful-

filled the relative distance criterion established by the ESEEM spectra (Fig. 3). RB1, which is the hydrogen bond between the malate hydroxyl group and the molecule of water coordinated to Mn, defines the juxtaposition of Mn to malate; conformers in which this angle varied over a range of 120° fulfilled the relative distance criterion established experimentally. However, RB2, the bond that defined the conformation of malate itself, i.e., the dihedral angle between the carboxyl groups, only varied within a range of 60°, and only four values of RB3 led to conformers that fulfilled the relative distance criterion. The conformation of malate itself is thus defined fairly closely, as shown in Figure 3. Within this family of conformers, the distance from Mn to H2 has a minimum value of 3.75 Å and a maximum value of 5.35 Å. This distance range may be compared with the distances between isocitrate and the divalent metal ion determined crystallographically in complexes with isocitrate dehydrogenase. In the Ca-isocitrate-ICDH complex, the distance between Ca and H2 is 4.1 Å (Stoddard et al., 1993), and in the Mg-isocitrate-ICDH complex, the Mg-H2 distance is 3.4 Å (Hurley et al., 1991). Therefore, the distances derived from the conformational search of Mn-malate complexes appear to be reasonable based on the precedents from analogous complexes defined crystallographically.

The interesting feature of the Mn-malate complexes that fulfill the distance constraints defined by the ESEEM data is that they have their carboxyl groups oriented *trans* to one another, suggesting that the enzyme does indeed bind the conformer that is most prevalent in solution. Modeling studies of active site complexes of isopropylmalate dehydrogenase, which also catalyzes a metal-dependent oxidative decarboxylation, led to the proposal that isopropylmalate also binds in the *trans* conformation (Zhang & Koshland, 1995). In contrast, complexes of isocitrate dehydrogenase with isocitrate show that isocitrate is bound in such a manner that, after oxidation, it will be oriented properly for decarboxylation (Hurley et al., 1991; Stoddard et al., 1993). Interestingly, it has been proposed that isopropylmalate dehydrogenase undergoes a conformational change after binding isopropylmalate (Zhang & Koshland, 1995), whereas no analogous substrate-induced conformational change is believed to occur with isocitrate dehydrogenase (Stoddard et al., 1993). In the case of malic enzyme, it remains to be determined at which stage in the catalytic cycle malate is adjusted to the conformation expected from stereoelectronic considerations, and whether that adjustment is a catalytically significant step.

Materials and methods

Chemicals

All chemicals and reagents were obtained from sources provided or prepared according to methods described previously (Karsten & Cook, 1994). The NAD-malic enzyme from *A. suum* was purified either by the method of Allen and Harris (1981) or that of Karsten and Cook (1994).

Synthesis of deuterated malate

Racemic 2-[^{2}H]malate was prepared by reducing OAA with NaB^2H_4 (98 atom%, Aldrich) as described before (Tipton, 1993). The resulting mixture of (*R*,*S*) 2-[^{2}H]malate was incubated with tartrate dehydrogenase, which catalyzes the oxidative decarboxylation of 2*R*-malate. The residual (2*S*)-[2-^{2}H]malate was purified by chromatography on Dowex AG1-x8 resin in the formate form. Fifteen micromoles of crude (2*S*)-[2-^{2}H]malate were applied to a 1.5 × 30-cm column equilibrated in water. The column was washed with 50 mL of water, and the malate was eluted with a 300-mL gradient from 0 to 4 M ammonium formate. Fractions were assayed for malate using malic enzyme; all fractions containing malate were pooled and concentrated by rotary evaporation. (2*S*)-[3*R*-^{2}H]malate was prepared enzymatically by the fumarase-catalyzed hydration of fumarate in D_2O. (2*S*)-[3*S*-^{2}H]malate was prepared enzymatically in two steps from [$^2H_2$]fumarate (MSD Isotopes, 98.2 atom% deuterium) (Blanchard & Cleland, 1980). Aspartase was used to catalyze the conversion of fumarate into aspartate, which was converted to malate by the sequential actions of glutamate-OAA transaminase and malate dehydrogenase. Both isotopomers of 3-[^{2}H]malate were purified before use by anion exchange chromatography, as described above. The isotopic composition of all three isotopomers of malate used in this study was determined by ^{1}H NMR; the incorporation of deuterium in each case was greater than 95%, and occurred exclusively at the expected positions.

ESEEM spectroscopy

Samples containing 250 μM malic enzyme active sites, 200 μM $MnSO_4$, and 3.4 mM deuterated or unlabeled malate were prepared in a total volume of 0.1 mL. Independent experiments performed with identical samples and analyzed by continuous wave EPR spectroscopy in quartz capillaries at room temperature demonstrated that all of the Mn^{2+} is bound to the enzyme under these conditions (Cohn & Townsend, 1954). Samples for ESEEM spectroscopy were prepared immediately before use, and were frozen in a stripline transmission cavity (Mims, 1974).

ESE modulation envelopes were obtained using a home-built spectrometer operating at X-band that has been described (McCracken et al., 1987). Care was taken to ensure that the data obtained for each sample were collected under identical conditions. The sample temperature was maintained at 2 K with a helium immersion dewar kept under reduced pressure. The magnetic field strength was 3,165 G and the microwave radiation frequency was 8.861 GHz. Stimulated echo modulation envelopes (Peisach et al., 1979) were collected; each pattern consisted of 1,024 data points, for which each point was the average of 50 measurements of the echo amplitude at that value of $T + \tau$, where T is the delay between the second and third microwave pulses, and τ is the delay between the first and second pulses. The repetition rate between pulse cycles was 101 Hz, and T was increased by 5 ns with each successive cycle. The value of τ was selected to minimize modulations arising from protons (Mims & Peisach, 1981).

Because the ^{2}H modulations were the only features of interest in these spectra, they were analyzed by dividing the spectrum obtained with the complex of malic enzyme and unlabeled malate into each spectrum obtained with the complex of malic enzyme and one of the isotopomers of ^{2}H-malate. The resulting difference spectra (Mims et al., 1984; Serpersu et al., 1988) were processed using dead-time reconstruction (Mims, 1984) and Fourier transformation.

Construction of the malate model

Malate was constructed using standard parameters in the Sybyl software program (Tripos, Inc.). The resulting structure was optimized using MOPAC 5.0 with the PM3 Hamiltonian (Stewart, 1989); the structure of the molecule after energy minimization was compared with the structure of a Mn-malate complex determined by X-ray crystallography (Van Havere et al., 1980). The average difference between the calculated bond lengths and experimental bond lengths was less than 0.05 Å, and the bond angles in the calculated and experimental structures agreed within 2 ° in most cases. Three models were constructed for evaluation of Mn-deuterium distances and are shown in Figure 2. Mn was treated as a dummy atom in the Sybyl program; the Mn-oxygen distance was selected using the crystallographically determined distance (Van Havere et al., 1980). In the first model, malate was treated as a bidentate ligand of Mn, in which the C1 carboxyl group and the C2 hydroxyl groups occupied Mn coordination sites. This model has one relevant rotatable bond, designated RB1, which is the C2-C3 bond. In the second model, malate was treated as a unidentate ligand coordinated to malate through the hydroxyl group at C2. This model contains two rotatable bonds, RB1, which is defined above, and RB2, which is the C2-OH bond of malate. In the third model, malate was treated as an outer sphere ligand of Mn by placing a Mn-coordinated H_2O molecule in position to interact with the C2 hydroxyl oxygen through a hydrogen bond. This model contains the two rotatable bonds defined above, and RB3, which is the hydrogen bond between the malate hydroxyl group and the water molecule coordinated to Mn. All three models were energy minimized before the conformational searches were conducted.

Acknowledgments

Supported by grants to P.F.C. from the National Institutes of Health (GM36799) and the Robert A. Welch Foundation (B-1031), by grants to J.P. from the National Institutes of Health (GM40168 and RR02583), and by a postdoctoral fellowship to P.A.T. (GM12081).

References

Allen BL, Harris BG. 1981. Purification of malic enzyme from *Ascaris suum* using NAD+-agarose. *Mol Biochem Parisitol 2*:367-372.

Blanchard JS, Cleland WW. 1980. Use of isotope effects to deduce the chemical mechanism of fumarase. *Biochemistry 19*:4506-4513.

Chen CY, Harris BG, Cook PF. 1988. Isotope partitioning for NAD-malic enzyme from *Ascaris suum* confirms a steady-state random kinetic mechanism. *Biochemistry 27*:212-219.

Coffino AR, Peisach J. 1992. Nuclear modulation effects in high spin electron systems with small zero-field splittings. *J Chem Phys 97*:3072-3091.

Cohn M, Townsend J. 1954. A study of manganous complexes by paramagnetic resonance absorption. *Nature 173*:1090-1091.

Grissom CB, Cleland WW. 1985. Use of intermediate partitioning to calculate intrinsic isotope effects for the reaction catalyzed by malic enzyme. *Biochemistry 24*:944-948.

Grissom CB, Cleland WW. 1986. Carbon isotope effects on the metal ion catalyzed decarboxylation of oxalacetate. *J Am Chem Soc 108*:5582-5583.

Grissom CB, Cleland WW. 1988. Isotope effect studies of chicken liver NADP malic enzyme: Role of the metal ion and viscosity dependence. *Biochemistry 27*:2927-2934.

Hermes JD, Roeske CA, O'Leary MH, Cleland WW. 1982. Use of multiple isotope effects to determine enzyme mechanisms and intrinsic isotope effects. Malic enzyme and glucose-6-phosphate dehydrogenase. *Biochemistry 21*:5106-5114.

Hsu RY. 1970. Mechanism of pigeon liver malic enzyme. *J Biol Chem 245*:6675-6682.

Hsu RY, Mildvan AS, Chang GZG, Fung FH. 1976. Mechanism of malic enzyme from pigeon liver. *J Biol Chem 251*:6574-6583.

Hurley JH, Dean AM, Koshland DE, Stroud RM. 1991. Catalytic mechanisms of $NADP^+$-D dependent isocitrate dehydrogenase: Implications from the structures of magnesium-isocitrate and $NADP^+$ complexes. *Biochemistry 30*:8671-8678.

Karsten WE, Cook PF. 1994. Stepwise versus concerted oxidative decarboxylation catalyzed by malic enzyme: A reinvestigation. *Biochemistry 33*: 2096-2103.

Karsten WE, Gavva SR, Park SH, Cook PF. 1995. Metal ion activator effects on intrinsic isotope effects for hydride transfer and decarboxylation in the reaction catalyzed by the NAD-malic enzyme from *Ascaris suum*. *Biochemistry 34*:3253-3260.

Kiick DM, Harris BG, Cook PF. 1986. Protonation mechanism and location of rate-determining steps for the *Ascaris suum* nicotinamide adenine dinucleotide-malic enzyme reaction from isotope effect and pH studies. *Biochemistry 25*:227-236.

Larsen RG, Halkides CJ, Redfield AG, Singel DJ. 1992. Electron spin-echo envelope modulation spectroscopy of Mn^{2+}·GDP complexes of N-*ras* p21 with selective ^{15}N labeling. *J Am Chem Soc 114*:9608-9611.

Larsen RG, Halkides CJ, Singel DJ. 1993. A geometric representation of nuclear modulation effects: The effects of high electron spin multiplicity on the electron spin echo envelope modulation spectra of Mn^{2+} complexes of N-*ras* p21. *J Chem Phys 98*:6704-6721.

McCracken J, Peisach J, Dooley DM. 1987. Cu(II) coordination chemistry of amine oxidases: Pulsed EPR studies of histidine imidazole, water, and exogenous ligand coordination. *J Am Chem Soc 109*:4064-4072.

Metz H, Küchler J, Böttcher R, Windsch W. 1982. 1H ENDOR investigations in tris-sarcosine-calcium chloride doped with manganese. *Chem Phys Lett 89*:351-355.

Mims WB. 1974. Measurement of the linear electric field effect in EPR using the spin echo method. *Rev Sci Instrum 45*:1583-1591.

Mims WB. 1984. Elimination of the dead-time artifact in electron spin-echo envelope spectra. *J Magn Reson 59*:291-306.

Mims WB, Davis JL, Peisach J. 1984. The accessibility of type I Cu(II) centers in laccase, azurin, and stellacyanin to exchangeable hydrogen and ambient water. *Biophys J 45*:755-766.

Mims WB, Davis J, Peisach J. 1990. The exchange of hydrogen ions and of water molecules near the active site of cytochrome *c*. *J Magn Res 86*: 273-292.

Mims WB, Peisach J. 1981. Electron spin echo spectroscopy and the study of metalloproteins. In: Berliner LJ, Reuben J, eds. *Biological magnetic resonance, vol 3*. New York: Plenum Press. pp. 213-263.

Mims WB, Peisach J, Davis JL. 1977. Nuclear modulation of the electron spin echo envelope in glassy materials. *J Chem Phys 66*:5536-5550.

Park SH, Harris BG, Cook PF. 1986. pH Dependence of kinetic parameters for oxalacetate decarboxylation and pyruvate reduction reactions catalyzed by malic enzyme. *Biochemistry 25*:3752-3759.

Park SH, Kiick, DM, Harris BG, Cook PF. 1984. Kinetic mechanism in the direction of oxidative decarboxylation for NAD-malic enzyme from *Ascaris suum*. *Biochemistry 23*:5446-5453.

Peisach J, Mims WB, Davis J. 1979. Studies of the electron-nuclear coupling between Fe(III) and ^{14}N in cytochrome P-450 and in a series of low spin heme compounds. *J Biol Chem 254*:12379-12389.

Peisach J, Mims WB, Davis J. 1984. Water coordination by heme iron in metmyoglobin. *J Biol Chem 259*:2704-2706.

Pollack RM. 1978. Decarboxylations of β-keto acids and related compounds. In: Gandour RD, Schowen RL, eds. *Transition states of biochemical processes*. New York: Plenum Press. pp 467-492.

Rosevear PR, Mildvan AS. 1989. Ligand conformations and ligand-enzyme interactions as studied by the nuclear Overhauser effect. *Methods Enzymol 177*:333-358.

Schimerlik MI, Grimshaw CE, Cleland WW. 1977. Determination of the rate-limiting steps for malic enzyme by the use of isotope effects and other kinetic studies. *Biochemistry 16*:571-576.

Serpersu EH, McCracken J, Peisach J, Mildvan AS. 1988. Electron spin echo modulation and nuclear relaxation studies of staphylococcal nuclease and its metal-coordinating mutants. *Biochemistry 27*:8034-8044.

Snetsinger PA, Cornelius JB, Clarkson RB, Bowman MK, Belford RL. 1988. Electron spin echo envelope modulation studies of natural abundance carbon-13 and aluminum-27 in two disordered systems. *J Phys Chem 92*:3696-3698.

Steinberger R, Westheimer FH. 1951. Metal ion-catalyzed decarboxylation: A model for an enzyme system. *J Am Chem Soc 73*:429-435.

Stewart JJP. 1989. Optimization of parameters for semiempirical methods II. Applications. *J Comput Chem 10*:221-264.

Stoddard BL, Dean A, Koshland DE. 1993. Structure of isocitrate dehydrogenase with isocitrate, nicotinamide adenine dinucleotide phosphate, and

calcium at 2.5 Å resolution: A pseudo-Michaelis ternary complex. *Biochemistry 32*:9310–9316.

Tang CL, Hsu RY. 1973. Reduction of α-oxo carboxylic acids by pigeon liver "malic" enzyme. *Biochem J*:287–291.

Thornton EK, Thornton ER. 1978. Scope and limitations of the concept of the transition state. In: Gandour RD, Schowen RL, eds. *Transition states of biochemical processes*. New York: Plenum Press. pp 1–76.

Tipton PA. 1993. Intermediate partitioning in the tartrate dehydrogenase-catalyzed oxidative decarboxylation of D-malate. *Biochemistry 32*:2822–2827.

Van Havere W, Lenstra ATH, Geise HJ. 1980. Structure of manganese(II) trihydrate and comparison with other malates. *Acta Crystallogr B 36*: 3117–3120.

Viega Salles JB, Ochoa S. 1950. Biosynthesis of dicarboxylic acids by carbon dioxide fixation. *J Biol Chem 187*:849–861.

Weiss PM, Gavva SR, Harris BG, Urbauer JC, Cleland WW, Cook PF. 1991. Multiple isotope effects with alternative dinucleotide substrate as a probe of the malic enzyme reaction. *Biochemistry 30*:5755–5763.

Zhang T, Koshland DE. 1995. Modeling substrate binding in *Thermus thermophilus* isopropylmalate dehydrogenase. *Protein Sci 4*:84–92.